AURORAL EMISSIONS AND INNER MAGNETOSPHERIC DYNAMICS DURING EARTH'S RESPONSE TO THE 28TH OCTOBER 2021 CORONAL MASS EJECTION

J. E. Waters[1], C. M. Jackman[2], D. K. Whiter[3], A. R. Fogg[2], L. Lamy[7,1], J. A. Carter[4], J. C. Coxon[5] L. Fryer[3], C. K. Louis[2], L. J. Paxton[6], C. Briand[7], B. Cecconi[7], K. Issautier[7], X. Bonnin[7], and P. Gallagher[2]

*Corresponding author: james.waters@lam.fr

Citation:

Waters et al., 2023, Auroral emissions and inner magnetospheric dynamics during Earth's response to the 28th October 2021 Coronal Mass Ejection, *in Planetary, Solar and Heliospheric Radio Emissions IX, edited by C. K. Louis, C. M. Jackman, G. Fischer, A. H. Sulaiman, P. Zucca, published by DIAS, TCD*, pp. 155–170, doi: 10.25546/104047

Abstract

On 28th October 2021 the Sun released a large Coronal Mass Ejection (CME) in Earth's direction. An X1.0 class solar flare and a rare ground level enhancement (GLE) were observed, along with bright solar radio bursts. Here we examine data from the near–Earth environment to investigate the terrestrial response to this solar event, using newly accessible Wind Auroral Kilometric Radiation (AKR) observations. The CME arrival is tracked at ∼1 AU using remote radio observations from Wind, along with *in–situ* interplanetary magnetic field (IMF) and solar wind measurements from OMNI. Geomagnetic activity is studied with SYM–H, SuperMAG and PC indices. The auroral response is monitored for the first time with Wind AKR

[1] *LAM, Pythéas, Aix Marseille Université, CNRS, CNES, Marseille, France*
[2] *School of Cosmic Physics, DIAS Dunsink Observatory, Dublin Institute for Advanced Studies, Dublin 15, Ireland*
[3] *Department of Physics and Astronomy, University of Southampton, Highfield Campus, Southampton, SO17 1BJ, UK*
[4] *Planetary Sciences Group, School of Physics and Astronomy, University of Leicester, Leicester, UK*
[5] *Department of Mathematics, Physics, and Electrical Engineering, Northumbria University, Newcastle Upon Tyne, UK*
[6] *Applied Physics Laboratory, John Hopkins University, Laurel, Maryland, USA*
[7] *Observatoire de Paris, LESIA, PSL Research University, CNRS, Sorbonne Université, University of Paris, Meudon, France*

observations from L1 (Lagrange point 1), UV auroral emissions and field–aligned current densities, exploring the AKR source location and inner magnetospheric dynamics. We thus quantify the timeline for solar wind–magnetosphere–ionosphere coupling and address the visibility of AKR sources from Wind's position on the dayside at L1.

1 Introduction

A CME was observed as a broad halo by STEREO–A (Kaiser, 2005) at 15:35 UT on 2021 Oct. 28th. It followed an X1.0 class solar flare emitted from the AR12887 region and the ejection of relativistic protons and electrons from the solar atmosphere. The solar protons (∼450 MeV) produced rare ground level enhancements (GLEs) at Earth and both have been the subject of detailed study (e.g., Papaioannou et al., 2022; Klein et al., 2022; Mishev et al., 2022; Martucci et al., 2023), while Yamasaki et al. (2022) modelled the active region to explore the solar flare generation. Accelerated electrons generated intense solar radio bursts across the spectrum of Type II to Type IV bursts (Klein et al., 2022). The CME was observed by the Large Angle Spectrometric Coronagraph (LASCO; Brueckner et al., 1995) C2 as a partial halo propagating towards the south. We use this opportune solar event, in the new rising phase of the solar cycle, to introduce the large suite of newly accessible dayside AKR observations to the current perspective on magnetospheric dynamics garnered by geomagnetic indices and other observations.

Using novel techniques (Waters et al., 2021; Fogg et al., 2022) it is now possible to select AKR from Wind/WAVES observations, albeit contingent on visibility constraints. Events such as the interplanetary CME (ICME) discussed here can be used as a chance to characterise these constraints and explore the utility of these AKR observations. As well as this, the IMF and plasma parameters can be measured continuously by Wind at its current upstream position. These give insight to the occurrence of dayside reconnection which precedes the transfer of open flux across the polar cap. Widely distributed magnetometer stations are used to measure the following disturbance, signalling intensified current systems and the onset of storms and substorms (Iyemori, 1990; Newell & Gjerloev, 2011). Global maps of field–aligned currents (FACs) allow study of average properties during important space weather events (e.g., Coxon et al., 2014; Motoba et al., 2015; Coxon et al., 2018; Shi et al., 2020). Electron precipitation along the same FACs produces the UV and optical aurora in the ionosphere, and can also produce source regions of AKR under certain conditions (e.g., Wu & Lee, 1979; Treumann, 2006), far above the ionosphere. These auroral emissions, monitored remotely, provide a comprehensive picture of the dynamics of the auroral acceleration region when accounting for complex viewing effects of AKR (Gurnett, 1974; Alexander & Kaiser, 1976; Mutel et al., 2008; Zhao et al., 2019).

In this study, we examine the response of the near–Earth environment with the aforementioned tools as the ICME passes. Novel observations of AKR made by Wind/WAVES from L1, 250 R_E from Earth, are presented for the first time (to the authors' knowledge) with both the Defense Meteorological Satellite Program Special Sensor Ultraviolet

Spectrographic Imager (DMSP SSUSI, Paxton et al. (1992)), and the Active Magnetosphere and Planetary Electrodynamics Response Experiment (AMPERE, Anderson et al. (2000); Anderson et al. (2021); Waters et al. (2001, 2020)). By these means, we aim to establish the use of L1 AKR observations for future, larger–scale studies using the latest tools of magnetospheric observations. Section 2 presents the observations made throughout the coupling timeline following the ICME: Section 2.1 describes the upstream solar wind conditions from OMNI (King & Papitashvili, 2005) following the arrival of the ICME at Earth, as well as the geomagnetic response using PC (Stauning, 2013) and SuperMAG (Gjerloev, 2012) geomagnetic indices, supplemented by Wind/WAVES AKR observations. Section 2.2 presents UV auroral observations and global field–aligned current measurements with the observed AKR to interpret the driving origin of the radio emission. Section 3 summarises the case study of the event.

2 Observations

2.1 Solar wind conditions and geomagnetic activity

Figure 1 shows a combination of remote sensing and *in–situ* data which illustrate the impact of the ICME at Earth, from its arrival at ∼21:00 UT on 29th Oct. 2021 and the subsequent 3 days. Wind/WAVES/RAD1 radio observations are shown in panel a), exhibiting solar Type III radio bursts that are characterised by bright emission with a drifting feature at lower frequencies. The intense Type III burst at 15:28 UT on 28th Oct. 2021 in Figure 1a coincides with the X1.0 class solar flare, and magnetic connection to the solar surface is shown with intense Langmuir waves at 16:20 UT (Klein et al., 2022). Panels b) and c) illustrate the IMF and solar wind conditions from OMNI. The IMF Y and Z components, shown in Figure 1b, reveal a clock angle rotation accompanied by significant fluctuations on a high amplitude field background; consistent with the passage of the ICME at 21:00 UT on 29th Oct. 2021 (e.g., Carter et al., 2020). This clock angle rotation is accompanied by a multi–step increase in solar wind dynamic pressure between 11:00 and 20:00 UT on 30th Oct. 2021 (Figure 1c). Noting that median P_{SW} values at 1 AU are of the order of several nPa (e.g., Fogg et al., 2022), a pressure enhancement around 10 nPa suggests a substantially compressed magnetosphere. This is confirmed by a rapid increase then decrease in SYM–H to negative values (Araki, 1994), here with oscillations around the negative peak at ∼05:00 UT, 31st Oct. 2021 in Figure 1d. This indicates a geomagnetic sudden storm commencement (SSC), driven by a rapid compression of the magnetosphere, in turn by CMEs (Taylor et al., 1994). This is followed by a disturbed recovery period in SYM–H.

Geomagnetic indices are powerful tools which characterise the state of the magnetosphere. SYM–H (Iyemori, 1990) is derived from magnetometers at equatorial latitudes, indicating changes in the ring current and shows characteristic signatures of geomagnetic storms (e.g., Walach & Grocott, 2019); seen in Figure 1d. In this section, PC(N,S), SMU and SML indices are used; all continuous, minute resolution products derived from ground–based magnetometer data, thus not limited by spacecraft position. Each index is amalgamated from various stations, and shows deflections in the magnetic field as a result of changes

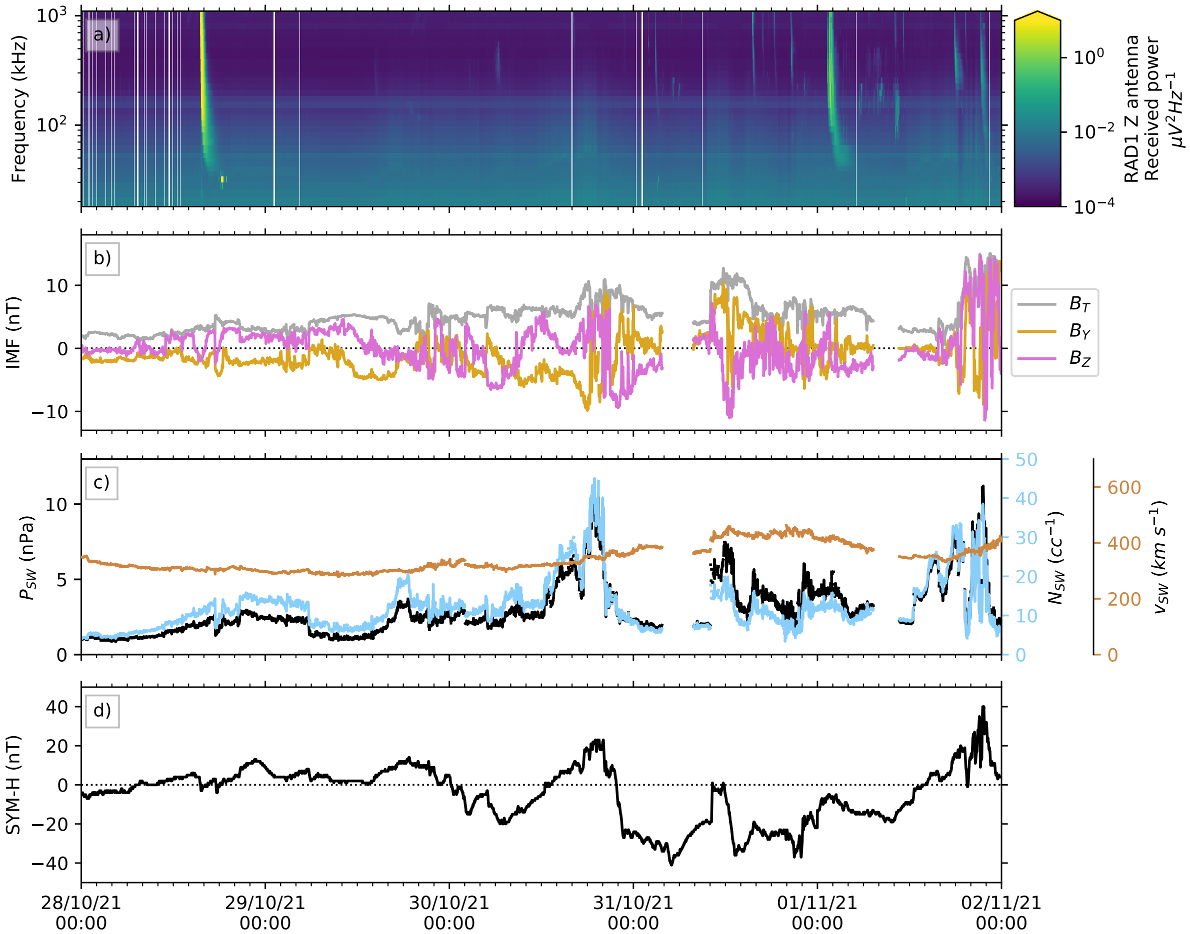

Figure 1: *Observations between the 28th Oct. and 2nd Nov. 2021 of: a) a frequency–time dynamic spectrogram showing received radio power between 20–1045 kHz, according to the scale on the right; b) total* B_T *(grey) and transverse* B_Y *(orange),* B_Z *(pink) IMF magnitudes; c) solar wind flow pressure* P_{SW} *(black), proton density* N_{SW} *(cyan) and flow speed* V_{SW} *(orange); d) SYM–H, showing the terrestrial ring current response.*

in overhead currents. The polar cap indices PC(N,S) (e.g., Troshichev & Andrezen, 1985; Stauning, 2013) are measured by stations at polar latitudes in the northern and southern (geographic) hemispheres; they record the strength of cross polar currents, with larger values suggesting faster anti–sunward flux transport. Finally, SMU and SML are the upper and lower envelopes of the SuperMAG (Gjerloev, 2012) electrojet index, and show the strength of the eastward and westward electrojets respectively; these are measured from magnetometers in the auroral zone.

Figure 2 shows several parameters which reveal the terrestrial magnetospheric response to the arrival of the ICME. Figure 2b shows the associated response in geomagnetic indices. PC(N) and PC(S) follow similar dynamics throughout, suggesting balanced flux transport in both hemispheres. Between 28th–30th Oct. values are close to the medians of their distributions (Fogg et al., 2022), while subsequent sharp enhancements follow periods of Southward, negative IMF Z component. These occur at approximately 06:00 UT of 30th Oct., prior to the main P_{SW} enhancement, 22:00 UT on 30th Oct., 12:00 UT and

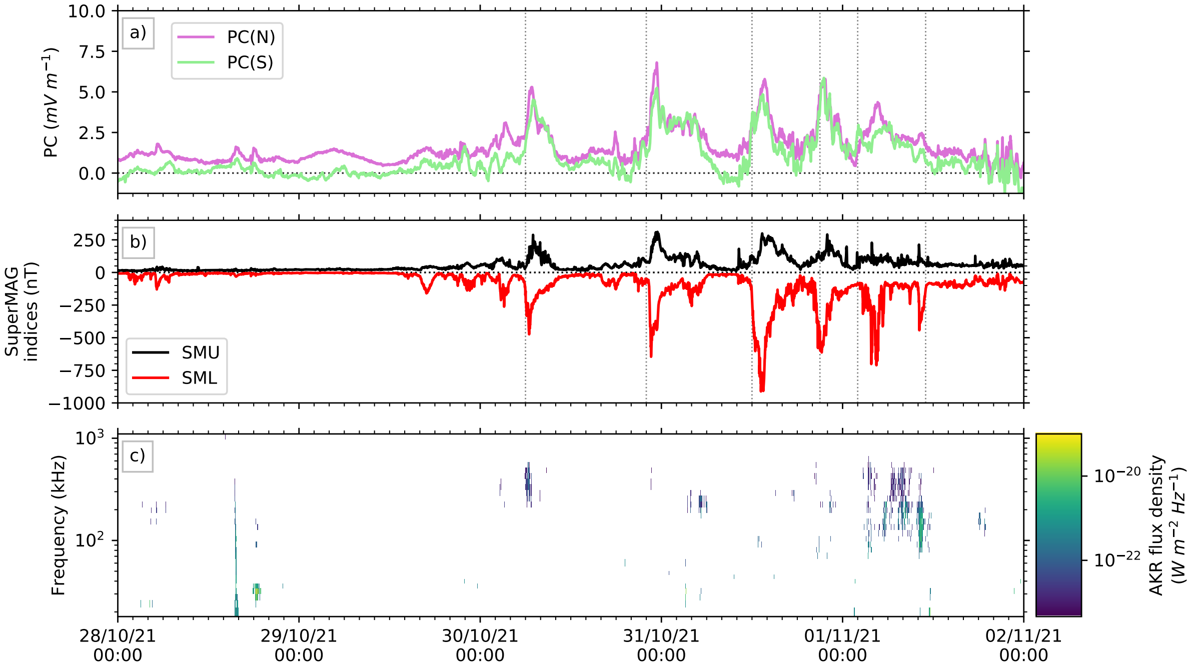

Figure 2: *Magnetospheric response given by a) the dayside reconnection rate, b) PC indices for both hemispheres, c) auroral electrojet (SMU/SML) indices from SuperMAG, d) AKR observations made from L1 and e) the SYM–H index for 28th Oct. to 2nd Nov. 2021. Vertical lines in panels a and b represent times of substorm onset (see text).*

21:00 UT on 31st Oct., and ∼03:00 UT on 1st Nov. 2021. The latter of these exhibits asymmetry that is atypical of this period; the peak PC(S) is ∼62% that of the peak PC(N) at ∼04:00 UT, and the PC(N) sees a more consistent increase. These enhancements evidence periods of rapid flux transport that facilitate the loading of magnetic energy, and are represented as vertical lines in Figure 2. This drives storm as well as substorm dynamics; we focus on the latter, presented in Figure 2b, in the following.

Substorms are a manifestation of various magnetospheric phenomena and represent an explosive release of energy between the outer and inner magnetosphere. They are studied with observational proxies from ground–based, remote sensing and *in–situ* instrumentation. Ground magnetometer station networks can measure the perturbation due to enhanced ionospheric currents. The SML index is a typical indicator of substorm onset; the substorm enhances the westward electrojet and hence shows a larger disturbance in the SML index, with sharp decreases indicating approximate onset time. When using SML values for identifying substorm onset by various means, Forsyth et al. (2015) found the largest of the median SML diversion was −200 nT, for the event list of Newell & Gjerloev (2011). Coxon et al. (2014) found that typical substorms have an average SML disturbance of −400 nT. "Supersubstorms" can produce diversions of −2700 nT in the AL index (Nishimura et al., 2020). This implies that multiple substorm–like events occur, with notable substorms of < -500 nT SML occurring within ∼1 hour of each PC index enhancement. An exception to this is at 10:00 UT on 1st Nov., where a substorm occurs with a −450 nT SML diversion alongside a much less prominent peak in the PC indices. This event is included as it coincides with the brightest AKR observation of the period. Each of these events has peak magnitudes for the SML index > 2 times that of the corresponding SMU index. The first of these large substorms occurs on 30th Oct. 2021 at ∼ 06:00 UT; around 39 hours after solar flares were recorded on the 28th Oct. 2021. The activity after 03:00 UT on 1st Nov. appears to be more complex than other notable substorms here, with multiple sharp decreases between 03:00 and 06:00 UT.

Although limited by viewing at L1, we display AKR observations in Figure 2d for context and aim to use them to infer further magnetospheric dynamics in the following section.

2.2 AKR, dayside aurora and field–aligned currents

This section explores the AKR observations in more detail with conjugate auroral and field–aligned current observations from DMSP SSUSI and AMPERE, respectively. The AKR observations in Figure 2d follow the application of the process described in Waters et al. (2021), and show sparse emission at typical AKR frequencies (100–700 kHz, Morioka et al. (2007, 2013)). The most significant AKR observations are made at frequencies 70–500 kHz, between 03:00–11:00 UT on 1st Nov., with the most intense burst observed between 70–240 kHz and corresponding to the final substorm at 10:00 UT.

The SSUSI instrument (Paxton et al., 1992) consists of a scanning spectrometer that observes the aurora in 5 wavelengths, capturing electron precipitation through their interaction with the ionosphere. As a DMSP spacecraft passes over the pole, taking ∼20 minutes, observations of segments perpendicular to the footpath of the satellite are made. For this analysis, SSUSI observations of auroral radiance and the corresponding position in the oval are binned over 15 seconds and averaged to give values representing a relatively small local area. We use data from the DMSP F18 spacecraft and the Lyman–Birge–Hopfield short channel (N_2 emission, 140–150 nm). To constrain the auroral location, SSUSI observations of the dayside oval are subset into 4 hour wide magnetic local time (MLT) sectors for each polar pass. Given the slight variation in spacecraft trajectory for each orbit and subsequent spatial sampling, each MLT sector for each orbit has a differing number of data included, also varying between orbits. As SSUSI orbital passes take 20 minutes, AKR and UV auroral emission cannot be quantified certainly on timescales less than this. Data in each sector are thus averaged, with the time set as the midpoint of the orbital pass.

Figure 3 shows a time series of auroral UV radiance in kR, using data from the SSUSI observations. Data have been reduced over each orbit of the DMSP F18 spacecraft for this period and subset in 06–10 hrs, 10–14 hrs and 14–18 hrs MLT sectors. Panels a) and b) show the mean averaged and 90th percentile values of the auroral radiances for each MLT sector. The afternoon sector (14–18 hrs) exhibits the brightest mean auroral radiance (Figure 3a) of the dayside for these observations, reaching the maximum of 0.39 kR following the largest substorm onset on 31st Oct. at 13:00 UT. Figure 3b represents extreme occurrences and likely the presence of bright, discrete aurora for values much higher than the mean. This is true for the afternoon sector where peak 90th percentile values are 2–3 times the mean values, and is confirmed from examination of the SSUSI polar projection plots (not included). Similar extreme values relative to the mean are

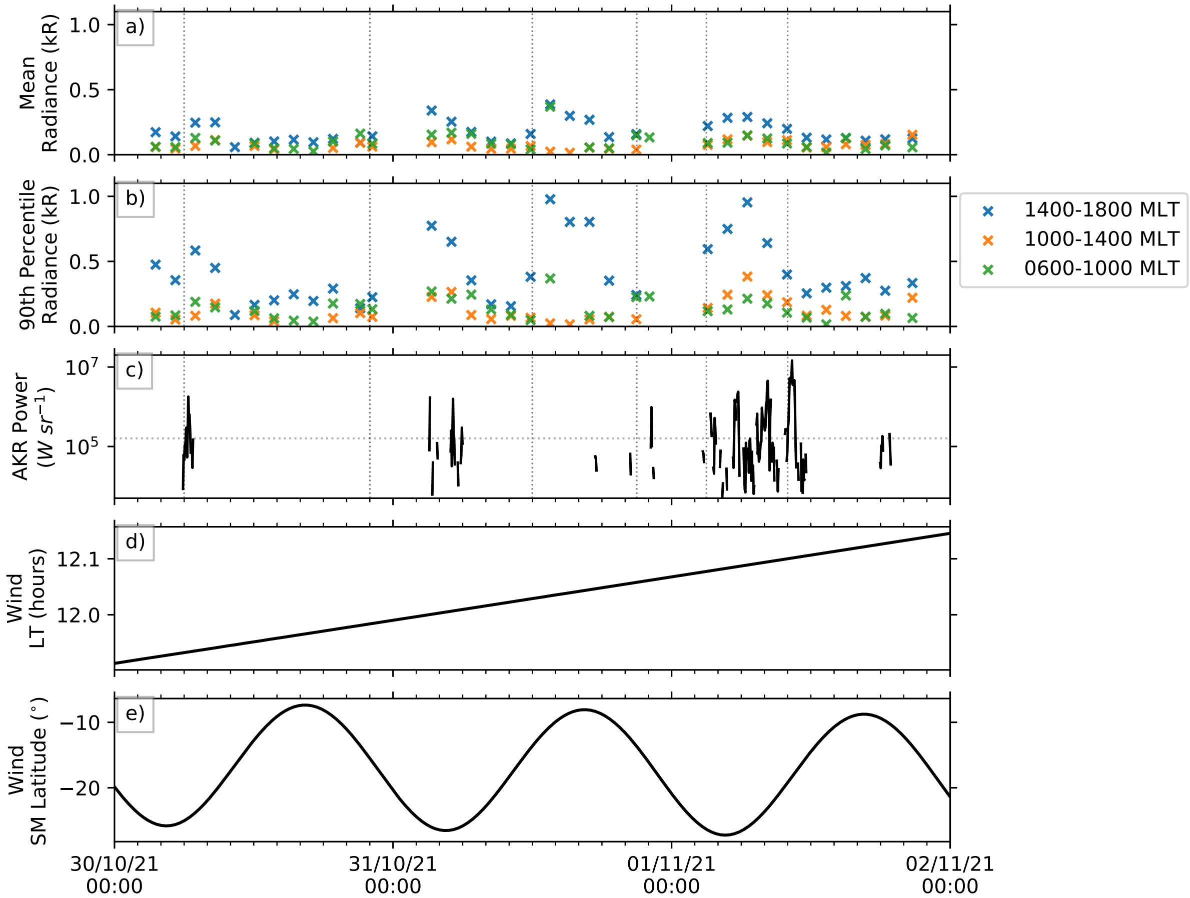

Figure 3: *a) Mean and b) 90th percentile of electron auroral radiances for 4 hour wide MLT sectors on the dayside, with each marker representing selected DMSP SSUSI observations. c) Fractional emitted AKR power from Wind/WAVES, integrated between 30–650 kHz. The faint horizontal line indicates the approximate 10 year (1995–2004) average at 12:00 LT from Waters et al. (2022). d) LT and e) latitude of Wind in the solar magnetic coordinate system.*

not seen in other MLT sectors, suggesting either diffuse aurora or a lack of data for those orbital passes.

Figure 3c shows the AKR power, integrated over frequencies 30–650 kHz from the observations in Figure 2c. Observed AKR bursts exhibit a peak power of $\sim 10^6\,\mathrm{W\,sr^{-1}}$ on average. The most intense burst, corresponding to the final substorm at 10:00 UT on 1st Nov., reaches $> 10^7\,\mathrm{W\,sr^{-1}}$, and is the last of a series of intensifications starting at 03:00 UT, the approximate time of the initial substorm of this day, with an apparent period of $\sim$ 2 hours. The average AKR power between 100–650 kHz observed by Wind during 1995–2004, and at 12 hrs LT, is $\sim 1\times10^5\,\mathrm{W\,sr^{-1}}$ (Waters et al., 2022). The bright, discrete aurora observed in the afternoon sector, with the exception of those at 13:00 UT on 31st Oct. 2021, are accompanied by AKR bursts. However, only 3 of 6 of the substorm events of note here occur with significant, $>$ 5 minute AKR bursts, namely the aforementioned AKR bursts and the burst at 06:00 UT on 30th Oct. As AKR source regions are usually found on the nightside and the beaming is highly directed, Wind cannot readily observe AKR from auroral substorms while it is at L1 (Mutel et al., 2008; Waters et al., 2021; Fogg et al., 2022). However, AKR sources can be more widely distributed in the dusk and dayside sectors depending on geomagnetic activity (Mutel et al., 2008; Zhao et al., 2019), and separate phenomena for dayside AKR sources such as cusp aurora and transpolar arcs exist (e.g., Alexander & Kaiser, 1977; Pedersen et al., 1992; Hanasz et al., 2000; Mutel et al., 2004).

Figures 3d and 3e give the local time (LT) and latitude of the Wind spacecraft, respectively, and in the geocentric solar ecliptic and solar magnetic (SM) coordinate systems. The former shows the slowly varying LT of Wind as it orbits L1, and the SM latitude varies as the magnetic dipole tilts with the diurnal rotation. Given that AKR sources exist on high latitude magnetic field lines, their broad emission cones will tilt with the magnetic axis as Earth rotates. Figures 3c and 3e show that, generally, AKR is observed from L1 when Wind is furthest from the magnetic equator. This agrees with previous studies of the effect of observer latitude on AKR viewing (Lamy et al., 2010; Waters et al., 2021), and is expected given the AKR beaming (Mutel et al., 2008). It would also explain the lack of observed AKR during the largest substorm at 13:00 UT on 31st Oct., with which the brightest auroral radiance is associated. However, given that the distance of Wind is so large at L1, 250 R_E away, and that the variation in magnetic latitude is relatively small at ~ 10 degrees, this question still stands and requires further statistical study with geometrical modelling, for example. However, it is clear that the observed AKR power is related to bright auroral structures between 14–18 hrs MLT. Previous mapping of AKR sources to discrete auroral structures (Huff et al., 1988; Menietti et al., 2011; Yearby & Pickett, 2022) and the presence of strong upward FACs required for their existence suggest this is the auroral source of the AKR, and the coincidence with substorm activity suggests these auroral structures are associated with the ionospheric current system that travels Westward at substorm onset.

This can be explored further in the context of the spatial distribution of field–aligned current (FAC) dynamics. For this, we use AMPERE data to compare with the most complete Wind AKR observations of the period, from 00:00–12:00 UT on 1st Nov 2021, covering the final two substorms considered. Choosing this period allows for the most informed analysis of these data given the qualitative scope of this study; in future we will return on a statistical basis. AMPERE (Anderson et al., 2000; Anderson et al., 2021; Waters et al., 2001, 2020) provides observations of upward and downward field–aligned current density, derived from magnetic perturbations measured aboard the Iridium telecommunication satellite network. If an upward FAC is present and dominates the downward FAC in magnitude, we assume that the surplus upward current density is governed by accelerated electrons that could provide the conditions for AKR source regions. The field–aligned current densities are presented in AACGM (Altitude–Adjusted Corrected GeoMagnetic) coordinates (Shepherd, 2014) on a grid extending over 50° of latitude and 24 hours of MLT, available for both the Northern and Southern hemispheres. AMPERE current densities are computed over a ten–minute–long sliding window, which is evaluated every two minutes. We integrate the field–aligned current densities to calculate the total upward and downward FACs, and we do this over six four–hour–wide MLT sectors on the dayside and nightside (which we split at the dawn–dusk meridian). In this way, we spatially quantify the FACs for the period in a similar way to the auroral radiance observed by SSUSI (Figure 3).

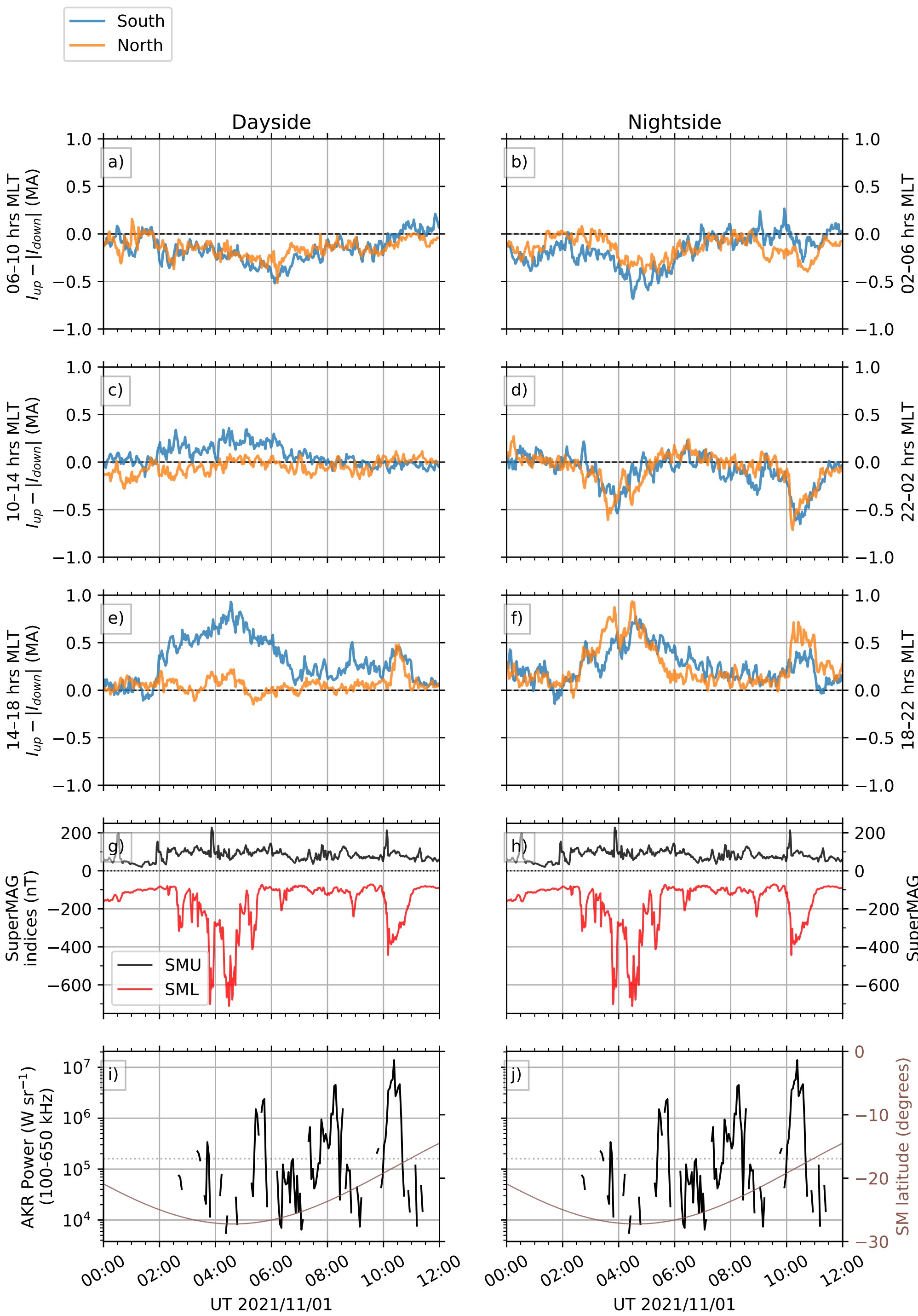

Figure 4: *Field–aligned current dynamics with AKR power for 12 hours (00:00–12:00 UT) of 1st Nov. 2021, during the most complete observations of AKR from Wind at L1 following the ICME discussed here. The AMPERE data are given in terms of the magnitude difference, in MA, of total upward and downward FACs over 4 hour wide MLT sectors as described in Section 2.2; the left column represents the magnetic dayside, showing MLT sectors between 0600–1800 hrs from top to bottom, while the right column shows nightside sectors between 1800–0600 hrs MLT, from bottom to top. SuperMAG SMU (in black) and SML (in red) indices are given in panels g and h. The AKR integrated power is duplicated in panels i and j and is shown with the spacecraft solar magnetic latitude on the right ordinate axis, as given in Figure 3e. The faint horizontal dashed lines indicate the approximate 10 year (1995–2004) average at 12:00 LT from Waters et al. (2022).*

Figure 4 illustrates the field–aligned current (FAC) dynamics in terms of the magnitude difference of total upward and downward FACs for each hemisphere; a positive value indicates dominant upward FACs while negative values indicate dominant downward FACs. The left column represents the magnetic dayside, showing MLT sectors between 06–18 hrs from top to bottom (panels a, c, e), while the right column shows nightside sectors between 1800–0600 hrs MLT, from bottom to top (panels b, d, f). We include the entire pole for the most general view and to check for other dayside FAC dynamics that could provoke AKR generation. The SuperMAG SMU and SML indices for this period are shown in Figures 4g and 4h for comparison. The AKR power is duplicated in panels i and j, with the solar magnetic latitude of Wind shown as in Figure 3e.

Considering the FAC dynamics in the dayside 14–18 hrs MLT sector (Figure 4e) and the nightside 18–22 hrs MLT sector (4f), there is a clear dominance of the upward FAC corresponding to both substorms. Following the initial substorm, at ∼ 03:00 UT, and for the the 14–18 hrs MLT sector, the upward FAC is much greater relative to downward FAC in the South than in the North. The upward FAC magnitude exceeds the downward FAC in the South considerably for ∼ 4 hours, which could be related to the continued sharp decreases in SML seen between 03:30 UT and 05:30 UT in Figure 4g. The difference between hemispheres in the FAC dynamics around 04:00 UT could be explained by the imbalanced PC(N) and PC(S) indices (Figure 2a), but we reserve further comment here. The second substorm at ∼ 10:00 UT is accompanied by dominant upward FACs in both hemispheres for these sectors. It should be noted that the peak magnitude of the upward FAC in 14–18 hrs MLT is ∼60% of that in the 18–22 hrs MLT sector for the Southern hemisphere, and approximately 34% in the Northern hemisphere, for this substorm.

In the nightside MLT sectors 22–02 hrs (Figure 4d) and 02–06 hrs (4b) in both hemispheres, downward FACs exceed upward FACs around substorm onsets on 1st Nov. This could indicate the closing of the auroral electrojet by the FACs, particularly the Westward substorm electrojet given the substorm activity following 30th Oct, and is most clear in the Figure 4d. The dayside MLT sectors of 06–14 hrs (Figures 4a and 4c), show no obvious correlation with substorm activity (as is expected), AKR bursts, or the dynamics of other MLT sectors. The FACs are generally balanced with discrepancies ∼ 25–50 % of those in other MLT sectors, suggesting a lack of appropriate conditions for AKR generation.

While the AKR bursts here appear to be periodic and increasing in power, they show no obvious correlation with the FAC dynamics. However, the increasing power could be due to the sustained upward FAC in the 14–18 hrs MLT sector. The bursts at ∼04:00 UT and ∼05:30 UT appear to correlate with decreases in the SML index, however. The final, most powerful AKR burst at 10:30 UT, appears to occur concurrently with peaks in the upward FACs in the 14–18 and 18–22 MLT sectors, demonstrating that the FACs during the second substorm show clear alignment with the AKR. However, the dominant FAC dynamics during the first substorm (∼04:00 UT) do not show a good correlation with the AKR.

While a stronger upward FAC suggests acceleration of electrons, this does not guarantee the plasma morphology for AKR generation. At Earth, a sustained parallel electric field is thought to be the primary method of acceleration to create the necessary plasma cavity (Ergun et al., 2000). Alfvénic acceleration may also contribute to the overall FAC dynamics, however. For this reason, it is likely that the enhanced upward FAC between ∼04:00–06:30 UT is comprised of both Alfvénic acceleration and that attributable to parallel electric fields, based on the AKR observations. However, given the clear excess of upward FACs in the duskside MLT sectors (14–18 hrs and 18–22 hrs MLT) compared to the pole in general we can be fairly certain that the AKR source is found in this MLT range. Also notable is the concurrence of the brightest auroral structures on the dayside (∼04:00 UT in Figure 3a) with the peak relative enhancement of upward FAC in the 14–18 hrs MLT sector, showing explicitly that while auroral brightening occurs from electron acceleration in general it cannot be a sole indicator of AKR occurrence. Conversely, the substorm at 10:00 UT sees clear enhancement of upward FAC that more closely follows the profile the most intense AKR burst observed. This implies that electron acceleration via sustained parallel electric field is the dominant mechanism in this instance, and the earlier event is accompanied by both this and Alfvénic acceleration.

3 Summary

An ICME that erupted from the Sun on 28th Oct. 2021 was accompanied by an X1.0 class solar flare and intense radio emissions, with SEPs (Solar Energetic Particles) producing GLEs measured at Earth. The associated magnetic structures rapidly induced an SSC geomagnetic storm when they reached Earth ∼ 2 days later, revealed in the OMNI solar wind observations and the SYM–H geomagnetic index. Using derivative measures of ground magnetometers in the PC and SuperMAG indices, we infer the presence of multiple substorm onsets following the initial IMF clock angle rotation at 21:00 on 29th Oct. 2021.

Novel observations of AKR by Wind at L1 are presented, that show bursts that exceed the 10 year average from the same LT by ∼ 1–2 orders of magnitude. Bursts are observed when Wind is further from the magnetic equator, suggesting a longitudinal and latitudinal viewing effect. SSUSI auroral observations show discrete aurorae in the afternoon sector that correlate with the AKR bursts. Using AMPERE data aggregated into MLT sectors for both the dayside and nightside, covering only the AKR bursts observed on 1st Nov., show dominant upward FACs on the duskside, between 1400–1800 hrs MLT. Visual correlation between the FAC dynamics and AKR bursts suggests the occurrence of both Alfvénic electron acceleration and acceleration due to double layer potential structures during the initial substorm of 1st Nov. at ∼04:00 UT, while the parallel electric fields dominate for the substorm at ∼11:00 UT. In this way, comparison of specific observations can give an insight into the acceleration processes that occur during FAC enhancements, and will precede the use of Wind's L1 AKR observations in the future.

The above suggests that the AKR source is highly likely to be within the MLT range 1400–2200 hrs, although the hemisphere of origin is still uncertain. Given the inner magnetospheric dynamics, inferred from the PC and SuperMAG indices as well as SSUSI and AMPERE data, the observed AKR enhancement seems to coincide with substorm dynamics and the associated electrojet morphology, namely the dominance of the Westward electrojet. Although comprehensively disentangling the effects of visibility and intrinsic source variability on the observations is out of the scope of this study, the comparison of these observational data allows for inferences to be made on the dominant auroral acceleration mechanism as well as the spatial structure, and precede the wider statistical use of Wind AKR observations from L1 that will be pursued in the future.

Acknowledgments

The authors acknowledge CNES (Centre National d'Etudes Spatiales), CNRS (Centre National de la Recherche Scientifique), and Observatoire de Paris for support to the Wind/Waves team and the CDPP (Centre de Données de la Physique des Plasmas) for the provision of the Wind/Waves RAD1 L2 data. The authors acknowledge support from Paris Astronomical Data Centre (PADC) for the preparation and distribution of the data collection. CMJ's, CKL's and ARF's work is supported by the Science Foundation Ireland Grant 18/FRL/6199. ARF's work was also supported by Irish Research Council Government of Ireland Postdoctoral Fellowship GOIPD/2022/782. DKW was supported by NERC IRF NE/S015167/1. JAC is supported by Royal Society grant DHF\R1\211068. LJP acknowledges support from AFOSR MURI Award 26–0201–51–62 and NASA TIMED GUVI Phase E operations, grant 80NSSC19K0244. We acknowledge use of NASA/GSFC's Space Physics Data Facility's OMNIWeb service, and OMNI data. We gratefully acknowledge the SuperMAG collaborators (`https://supermag.jhuapl.edu/info/?page=acknowledgement`).

References

Alexander J. K., Kaiser M. L., 1976, Terrestrial kilometric radiation, 1. Spatial structure studies, *Journal of Geophysical Research*, *81, 5948*

Alexander J. K., Kaiser M. L., 1977, Terrestrial kilometric radiation, 2. Emission from the magnetospheric cusp and dayside magnetosheath, *Journal of Geophysical Research*, *82, 98*

Anderson B. J., Takahashi K., Toth B. A., 2000, Sensing global Birkeland currents with iridium® engineering magnetometer data, *Geophysical Research Letters*, *27, 4045*

Anderson B. J., Angappan R., Barik A., Vines S. K., Stanley S., Bernasconi P. N., Korth H., Barnes R. J., 2021, Iridium Communications Satellite Constellation Data for Study of Earth's Magnetic Field, *Geochemistry, Geophysics, Geosystems*, *22, e09515*

Araki T., 1994, *in A Physical Model of the Geomagnetic Sudden Commencement, eds Engebretson, M. J. and Takahashi, K. and Scholer, M.*, American Geophysical Union, Washington, D.C., pp 183–200, doi:10.1029/GM081, `http://doi.wiley.com/10.1029/GM081p0183http://doi.wiley.com/10.1029/GM081`

Brueckner G. E., et al., 1995, The Large Angle Spectroscopic Coronagraph (LASCO), *Solar Physics*, *162, 357*

Carter J. A., Milan S. E., Fogg A. R., Sangha H., Lester M., Paxton L. J., Anderson B. J., 2020, The Evolution of Long-Duration Cusp Spot Emission During Lobe Reconnection With Respect to Field-Aligned Currents, *Journal of Geophysical Research (Space Physics)*, *125, e27922*

Coxon J. C., Milan S. E., Clausen L. B., Anderson B. J., Korth H., 2014, A superposed epoch analysis of the regions 1 and 2 Birkeland currents observed by AMPERE during substorms, *Journal of Geophysical Research (Space Physics)*, *119, 9834*

Coxon J. C., Milan S. E., Anderson B. J., 2018, A Review of Birkeland Current Research Using AMPERE, *in Electric Currents in Geospace and Beyond, eds Keiling A., and Marghitu O., and Wheatland M.*, pp 257–278, doi:10.1002/9781119324522.ch16

Ergun R. E., Carlson C. W., McFadden J. P., Delory G. T., Strangeway R. J., Pritchett P. L., 2000, Electron-cyclotron maser driven by charged-particle acceleration from magnetic field-aligned electric fields, *The Astrophysical Journal*, *538, 456*

Fogg A. R., Jackman C. M., Waters J. E., Bonnin X., Lamy L., Cecconi B., 2022, Wind/WAVES observations of Auroral Kilometric Radiation: automated burst detection and terrestrial solar wind–magnetosphere coupling effects, *Journal of Geophysical Research (Space Physics)*, *127, e30209*

Forsyth C., Rae I. J., Coxon J. C., Freeman M. P., Jackman C. M., Gjerloev J., Fazakerley A. N., 2015, A new technique for determining Substorm Onsets and Phases from Indices of the Electrojet (SOPHIE), *Journal of Geophysical Research (Space Physics)*, *120, 10,592*

Gjerloev J. W., 2012, The SuperMAG data processing technique, *Journal of Geophysical Research (Space Physics)*, *117, A09213*

Gurnett D. A., 1974, The Earth as a radio source: Terrestrial kilometric radiation, *Journal of Geophysical Research*, *79, 4227*

Hanasz J., Boudjada M. Y., Schreiber R., Krawczyk Z., Malycha M., Mogilevsky M. M., Rucker H. O., Romantsova T. V., 2000, Dynamic spectra of the Stokes parameters for the dayside and nightside auroral kilometric radiation, *Geophysical Research Letters*, *27, 1631*

Huff R. L., Calvert W., Craven J. D., Frank L. A., Gurnett D. A., 1988, Mapping of auroral kilometric radiation sources to the aurora, *Journal of Geophysical Research*, *93, 11445*

Iyemori T., 1990, Storm-time magnetospheric currents inferred from mid-latitude geomagnetic field variations, *Journal of Geomagnetism and Geoelectricity*, *42, 1249*

Kaiser M. L., 2005, The STEREO mission: an overview, *Advances in Space Research*, *36, 1483*

King J. H., Papitashvili N. E., 2005, Solar wind spatial scales in and comparisons of hourly Wind and ACE plasma and magnetic field data, *Journal of Geophysical Research (Space Physics)*, *110, 2104*

Klein K.-L., et al., 2022, The relativistic solar particle event on 28 October 2021: Evidence of particle acceleration within and escape from the solar corona, *Astronomy & Astrophysics*, *663, A173*

Lamy L., Zarka P., Cecconi B., Prangé R., 2010, Auroral kilometric radiation diurnal, semidiurnal, and shorter-term modulations disentangled by Cassini, *Journal of Geophysical Research (Space Physics)*, *115, A09221*

Martucci M., et al., 2023, The First Ground-Level Enhancement of Solar Cycle 25 as Seen by the High-Energy Particle Detector (HEPD-01) on Board the CSES-01 Satellite, *Space Weather*, *21, e2022SW003191*

Menietti J. D., Mutel R. L., Christopher I. W., Hutchinson K. A., Sigwarth J. B., 2011, Simultaneous radio and optical observations of auroral structures: Implications for AKR beaming, *Journal of Geophysical Research (Space Physics)*, *116, A12219*

Mishev A. L., Kocharov L. G., Koldobskiy S. A., Larsen N., Riihonen E., Vainio R., Usoskin I. G., 2022, High-Resolution Spectral and Anisotropy Characteristics of Solar Protons During the GLE N°73 on 28 October 2021 Derived with Neutron-Monitor Data Analysis, *Solar Physics*, *297, 88*

Morioka A., et al., 2007, Dual structure of auroral acceleration regions at substorm onsets as derived from auroral kilometric radiation spectra, *Journal of Geophysical Research (Space Physics)*, *112, A06245*

Morioka A., Miyoshi Y., Kurita S., Kasaba Y., Angelopoulos V., Misawa H., Kojima H., McFadden J. P., 2013, Universal time control of AKR: Earth is a spin-modulated variable radio source, *Journal of Geophysical Research (Space Physics)*, *118, 1123*

Motoba T., et al., 2015, On the formation and origin of substorm growth phase/onset auroral arcs inferred from conjugate space-ground observations, *Journal of Geophysical Research (Space Physics)*, *120, 8707*

Mutel R. L., Gurnett D. A., Christopher I. W., 2004, Spatial and temporal properties of AKR burst emission derived from Cluster WBD VLBI studies, *Annales Geophysicae*, *22, 2625*

Mutel R. L., Christopher I. W., Pickett J. S., 2008, Cluster multispacecraft determination of AKR angular beaming, *Geophysical Research Letters*, *35, L07104*

Newell P. T., Gjerloev J. W., 2011, Evaluation of SuperMAG auroral electrojet indices as indicators of substorms and auroral power, *Journal of Geophysical Research (Space Physics)*, *116, A12211*

Nishimura Y., et al., 2020, Extreme magnetosphere–ionosphere–thermosphere responses to the 5 April 2010 supersubstorm, *Journal of Geophysical Research (Space Physics), 125, e27654*

Papaioannou A., et al., 2022, The first ground level enhancement of solar cycle 25 on 28 October 2021, *Astronomy and Astrophysics, 71, L5*

Paxton L. J., et al., 1992, Special Sensor Ultraviolet Spectrographic Imager: An Instrument Description, *Instrumentation for Planetary and Terrestrial Atmospheric Remote Sensing, 1745, 2*

Pedersen B. M., Pottelette R., Eliasson L., Murphree J. S., Elphinstone R. D., Bahnsen A., Jespersen M., 1992, Auroral kilometric radiation from transpolar arcs, *Journal of Geophysical Research, 97, 10567*

Shepherd S. G., 2014, Altitude-adjusted corrected geomagnetic coordinates: Definition and functional approximations, *Journal of Geophysical Research (Space Physics), 119, 7501*

Shi Y., Knipp D. J., Matsuo T., Kilcommons L., Anderson B., 2020, Event studies of high-latitude FACs with inverse and assimilative analysis of AMPERE magnetometer data, *Journal of Geophysical Research (Space Physics), 125, e27266*

Stauning P., 2013, The Polar Cap index: A critical review of methods and a new approach, *Journal of Geophysical Research (Space Physics), 118, 5021*

Taylor J. R., Lester M., Yeoman T. K., 1994, A superposed epoch analysis of geomagnetic storms, *Annales Geophysicae, 12, 612*

Treumann R. A., 2006, The electron-cyclotron maser for astrophysical application, *Astronomy and Astrophysics Review, 13, 229*

Troshichev O. A., Andrezen V. G., 1985, The relationship between interplanetary quantities and magnetic activity in the southern polar cap, *Planetary and Space Science, 33, 415*

Walach M. T., Grocott A., 2019, SuperDARN Observations During Geomagnetic Storms, Geomagnetically Active Times, and Enhanced Solar Wind Driving, *Journal of Geophysical Research (Space Physics), 124, 5828*

Waters C. L., Anderson B. J., Liou K., 2001, Estimation of global field aligned currents using the iridium® System magnetometer data, *Geophysical Research Letters, 28, 2165*

Waters C. L., Anderson B. J., Green D. L., Korth H., Barnes R. J., Vanhamäki H., 2020, Science data products for ampere, *in Ionospheric Multi-Spacecraft Analysis Tools: Approaches for Deriving Ionospheric Parameters, eds Dunlop, Malcolm Wray and Lühr, Hermann*, Springer International Publishing, Cham, pp 141–165, doi:10.1007/978-3-030-26732-2˙7, `https://doi.org/10.1007/978-3-030-26732-2_7`

Waters J. E., Jackman C. M., Lamy L., Cecconi B., Whiter D. K., Bonnin X., Issautier K., Fogg A. R., 2021, Empirical selection of Auroral Kilometric Radiation during a multipoint remote observation with Wind and Cassini, *Journal of Geophysical Research (Space Physics)*, *126, e29425*

Waters J. E., et al., 2022, A perspective on substorm dynamics using 10 years of Auroral Kilometric Radiation observations from Wind, *Journal of Geophysical Research (Space Physics)*, *127, e30449*

Wu C. S., Lee L. C., 1979, A theory of the terrestrial kilometric radiation, *The Astrophysical Journal*, *230, 621*

Yamasaki D., Inoue S., Bamba Y., Lee J., Wang H., 2022, A data-constrained magnetohydrodynamic simulation of the X1.0 solar flare of 2021 October 28, *Astrophysical Journal*, *940, 119*

Yearby K. H., Pickett J. S., 2022, A review of cluster wideband data multi-spacecraft observations of auroral kilometric radiation, *Journal of Geophysical Research (Space Physics)*, *127, e2021JA029499*

Zhao W., Liu S., Zhang S., Zhou Q., Yang C., He Y., Gao Z., Xiao F., 2019, Global Occurrences of Auroral Kilometric Radiation Related to Suprathermal Electrons in Radiation Belts, *Geophysical Research Letters*, *2, 7230*